AN AMPLITUDE AND TRAVELTIME CALCULATION USING A HIGHER-ORDER PARABOLIC EQUATION

Ningya Cheng

Earth Resources Laboratory
Department of Earth, Atmospheric, and Planetary Sciences
Massachusetts Institute of Technology
Cambridge, MA 02139
and
Earth and Environmental Sciences Division
Mail Stop D443
Los Alamos National Laboratory
Los Alamos, NM 87545

Leigh House and Michael C. Fehler

Earth and Environmental Sciences Division
Mail Stop D443
Los Alamos National Laboratory
Los Alamos, NM 87545

ABSTRACT

A higher-order parabolic equation is used to compute the traveltime (phase) and the amplitude in constant density acoustic media. This approach is in the frequency domain, thereby avoiding the high frequency approximation inherent in the Eikonal equation. Intrinsic attenuation can be naturally incorporated into the calculation. The error at large angles of propagation caused by the expansion of the square root operator can be virtually eliminated by adding more terms to the expansion. An efficient algorithm is obtained by applying the alternate direction method. Our results are in excellent agreement with the finite element approach for the range-dependent wedge-shaped benchmark problem. The amplitude and the phase are calculated for a syncline and the Marmousi models.

INTRODUCTION

Numerical traveltime calculations are of great interest in exploration seismology. Traveltimes are crucial for the prestack seismic migration process. Finite difference schemes are the most computationally efficient traveltime methods (Vidale, 1988; Podvin and Lecomte, 1991; van Trier and Symes, 1991). These schemes are based upon the Eikonal equation, which is a high frequency approximation. However, finite difference schemes provide no amplitude information. The problems caused by using these first arrival times for imaging in complex velocity structures are discussed by Geoltrain and Brac (1993) and Nichols (1994).

The parabolic approximation to wave equations is widely used in seismic migration processing (Claerbout, 1985); an example is the 45-degree migration. It is based on the continued fraction expansion of a square root operator. Difficulty with the higher-order differential equation resulting from the higher-order expansion limits its practical application to second order terms. The parabolic approximation is seldom used for forward modeling in exploration seismology. On the other hand, in the field of ocean acoustics the parabolic equation is the main tool for forward modeling (Jensen *et al.*, 1994). The technique is well developed and widely used.

The purpose of this paper is to demonstrate the use of a higher-order parabolic equation to compute the phase (traveltimes) and amplitudes in a complex velocity structure. With a higher-order Padé series expansion, the angle limitation of one-way propagation is virtually eliminated. The traveltimes and amplitudes are computed in the frequency domain and the high frequency approximation is removed. Since amplitudes are important for reliable imaging, intrinsic attenuation becomes an important factor. Attenuation can be naturally and easily incorporated into our frequency domain calculation. The calculated phase (traveltime) can be used directly in the common shot prestack migration. The phase term from the source to the imaging point can be used as the imaging condition to form the migrated section. The amplitude information can be added as a weight to this imaging condition. In the following section, the higher-order parabolic equation is derived and the numerical implementation is described. Finally, the phases and amplitudes of a simple syncline and the Marmousi model (Bourgeois *et al.*, 1991) are calculated as numerical examples.

HIGHER-ORDER PARABOLIC EQUATION

In this section, we briefly derive the higher-order acoustic parabolic equation and describe its numerical solution method. In cylindrical coordinates (r, ϕ, z) for a media with constant density and azimuthal symmetry, the Helmholtz equation at frequency ω is:

$$\frac{\partial^2 p}{\partial r^2} + \frac{1}{r}\frac{\partial p}{\partial r} + \frac{\partial^2 p}{\partial z^2} + k_0^2 n^2 p = 0, \tag{1}$$

where $p(r,z)$ is the pressure, $k_0 = \omega/c_0$ is a reference wavenumber, and $n(r,z) = c_0/c(r,z)$ is the index of refraction; $c(r,z)$ is the velocity. The cylindrical coordinate r is pointed downward (Figure 1). Here, we are concerned with amplitudes as well as phases (traveltimes). From the traveltime point of view, a point source and a line source are identical. However, a point source and a line source will give very different amplitudes. Thus, the 2.5-D approach (cylindrical coordinates) is adopted to model the point source. We assume the solution takes the form:

$$p(r,z) = w(r,z)H_0^{(1)}(k_0 r), \tag{2}$$

where $H_0^{(1)}$ is the Hankel function. The envelope function $w(r,z)$ is assumed to be slowly varying in r. Substituting Equation (2) into Equation (1) and using the Hankel-function property and the far field assumption $k_0 r \gg 1$, we obtain:

$$\frac{\partial^2 w}{\partial r^2} + 2ik_0\frac{\partial w}{\partial r} + \frac{\partial^2 w}{\partial z^2} + k_0^2(n^2-1)w = 0, \tag{3}$$

where $i = \sqrt{-1}$. Factoring Equation (3) into an outgoing and an incoming wave component and keeping only the outgoing term we have:

$$\frac{\partial w}{\partial r} = ik_0\sqrt{(n^2 + \frac{1}{k_0^2}\frac{\partial^2}{\partial z^2} - 1)}w. \tag{4}$$

This is a one-way wave equation and is evolutionary in r. Keep in mind the approximation that backscattering is negligible. This is because the incoming wave term was dropped. We expand the square-root operator by a Padé series (Ma, 1982; Bamberger *et al.*, 1988),

$$\frac{\partial w}{\partial r} = ik_0\{\sum_{j=1}^{m}\frac{a_{j,m}(n^2 - 1 + \frac{1}{k_0^2}\frac{\partial^2}{\partial z^2})}{1 + b_{j,m}(n^2 - 1 + \frac{1}{k_0^2}\frac{\partial^2}{\partial z^2})}\}w \tag{5}$$

where coefficients $a_{j,m}$ and $b_{j,m}$ are

$$\begin{aligned} a_{j,m} &= \frac{2}{2m+1}\sin^2(\frac{j\pi}{2m+1}) \\ b_{j,m} &= \cos^2(\frac{j\pi}{2m+1}). \end{aligned} \tag{6}$$

The error caused by expansion of the square-root operator into a Padé series is plotted in Figure 2. With one term, the expansion is accurate to a propagation angle of about 40 degrees. By using seven terms in the expansion, the result is accurate for propagation angles up to 80 degrees. With more terms added to the expansion, the error associated

with the propagation direction can be virtually eliminated. Equation (5) can be solved by the method of alternating directions. This method requires the numerical solution of each term of the Padé series (Collins, 1989):

$$\frac{\partial w}{\partial r} = ik_0\{\frac{a_{j,m}(n^2 - 1 + \frac{1}{k_0^2}\frac{\partial^2}{\partial z^2})}{1 + b_{j,m}(n^2 - 1 + \frac{1}{k_0^2}\frac{\partial^2}{\partial z^2})}\}w. \tag{7}$$

The above equation is discretized in r by the Crank-Nicolson finite difference scheme. We obtain:

$$[1 + (b_{j,m} - \frac{i}{2}k_0\Delta r a_{j,m})(n^2 - 1 + \frac{1}{k_0^2}\frac{\partial^2}{\partial z^2})]w(r + \Delta r, z) = \tag{8}$$
$$[1 + (b_{j,m} + \frac{i}{2}k_0\Delta r a_{j,m})(n^2 - 1 + \frac{1}{k_0^2}\frac{\partial^2}{\partial z^2})]\bar{w}(r, z).$$

Then, the second-order derivative in z is discretized by second-order centered finite difference. This results in a tridiagonal linear system, which can be solved efficiently by forward and back substitution.

The advantage of the parabolic wave equation is that it can be solved by a marching method. However, this requires specification of the initial condition at $w(r_0, z)$ and boundary conditions. In this paper Greene's source is used as an initial condition (Greene, 1984).

$$w(0, z) = \sqrt{k_0}(1.4467 - 0.4201k_0^2(z - z_s)^2)e^{-\frac{k_0^2(z - z_s)^2}{3.0512}}, \tag{9}$$

which is a weighted Gaussian source. It simulates a point source and is ideal for use with the wide-angle parabolic equation. For the boundary condition we add an artificial absorbing layer to ensure that no significant energy is reflected back from the boundary.

NUMERICAL EXAMPLES OF PHASE (TRAVELTIME) AND AMPLITUDE

To make a quality assessment, the range-dependent benchmark problem solicited by the Acoustic Society of America in 1987 is considered (Jensen and Ferla, 1990). The wedge-shaped ocean model (case III) is tested. The ocean sound speed is 1500 m/s, and the ocean depth decreases from 200 m to zero over a distance of 4 km from the source. The surface is a free surface. A 25 Hz point source is located 100 m below the free surface. The half-space sediment sound speed is 1700 m/s and attenuation is 0.5

dB/λ. The attenuation is included in the calculation by adding a small imaginary part to the media wave wavenumber:

$$k = \frac{\omega}{c} + i\alpha. \tag{10}$$

The density is assumed constant for the test. The free surface is treated by requiring $w = 0$. The results are compared with the finite element solution given by Collins (1990). The transmission loss for the pressure receivers at depth 30 m and 150 m are plotted in Figure 3. The transmission loss is defined as:

$$TL = -10 \log_{10} \frac{I}{I_0}, \tag{11}$$

where I is the intensity at a field point and I_0 is the intensity 1 m from the source. Our method gives excellent agreement with the finite element scheme. The computational time on a SUN SPARC 10 workstation is plotted in Figure 4. The test model grid size is 250 × 350. The plot shows that the computational cost is directly proportional to the number of terms in the expansion. Higher accuracy is achieved with the cost of additional computing time.

We now show two examples of phase and amplitude calculations. The first is a simple two-layer syncline model (Figure 5a). The top layer velocity is 1500 m/s and the bottom layer velocity is 2000 m/s. There is no free surface in this case. The source frequency is 200 Hz and the grid size is 1 meter. Absorbing layers are used on both sides of the model to reduce boundary reflections. Phase and amplitude are plotted in Figures 5b and 5c, respectively. A total of 20 terms of the Padé expansion were used in the calculations. The wavefields near zero depth are not accurate due to the limited number of terms in the expansion. On both sides of the syncline only direct arrivals are observed. From the Eikonal solution (Cheng and House, 1995) the head waves generated from the interface can be seen along each side of the syncline (Figure 5d). These head waves usually have little energy. The head waves are not seen in our results because the parabolic equation only allows the waves to propagate in one direction. The amplitudes underneath the interface are low. This is because of the large incident angle which results in most energy being reflected back. A complex interference pattern is observed in the lower part of the syncline, which cannot be obtained by solving the Eikonal equation (geometric ray). This pattern is a direct result of the finite frequency nature of the parabolic equation solution (200 Hz). The pattern can be more easily seen on the amplitude result than on the phase result. Finally, note the caustic beneath the syncline. The caustic is very clear from the Eikonal solution, however the finite frequency solution gives a smoothed version of the caustic. As the distance increases away from the bottom of the syncline the caustic breaks into two parts.

Next, the Marmousi model is considered (Bourgeois *et al.*, 1991). This complicated model was created to test prestack migration algorithms. The square of the index of refraction is plotted in Figure 6a. A source frequency of 10 Hz and a grid size of 10 meters

are used in the calculation. The phase and the amplitude are plotted in Figures 6b and 6c. Because of the complexity of the model, it is hard to explain the phase and amplitude plots. The main features of the amplitude plot are the high amplitude channels. These channels carry more energy to the left side than to the right. This is because the normal faults that outcrop near the distance 5 km block energy transmission to the right. The phase plot shows many discontinuities, which underscore the complexity of the model.

CONCLUSIONS

In this paper, we use a higher-order parabolic equation to calculate phase (traveltimes) and amplitudes in a constant density acoustic media. The models all assume a point source. The calculated results (both phase and amplitudes) can be used for prestack migration. The higher-order parabolic equation approach is carried out in the frequency domain. The high frequency approximation inherent to the Eikonal equation is avoided. The parabolic equation approach also provides accurate amplitude information. Intrinsic attenuation can be naturally incorporated into the calculations. The errors at large angles of propagation that result from the expansion of the square-root operator can be virtually eliminated by adding more terms to the expansion. An efficient computational algorithm is obtained by applying the alternate direction method.

ACKNOWLEDGMENTS

We thank the Los Alamos National Laboratory's Laboratory-Directed Research and Development Program for supporting this work. This was performed under the auspices of the U.S. Department of Energy. One author (N. C.) was partially supported by ERL/MIT as a Postdoctoral Fellow.

REFERENCES

Bamberger, A., Engquist, B., Halpern, L. and Joly, P., 1988, Higher order parabolic wave equation approximation in heterogeneous media, *SIAM J. Appl. Math., 48,* 129-154.

Bourgeois, A., Bourget, M., Lailly, P., Ricarte, P., and Versteeg, R., 1991, Marmousi—The model and the data, *The Marmousi Experience*, Eur. Assn. Expl. Geophys., In Versteeg, R. and Grau, G., Eds.

Cheng, N. and House, L., 1995, Minimum traveltime calculation in 3D by graph theory, Submitted to *Geophysics.*

Claerbout, J.F., 1985, *Imaging the Earth's Interior,* Blackwell Scientific Publications.

Collins, M.D., 1989, Applications and time-domain solution of higher-order parabolic equation in underwater acoustics, *J. Acoust. Soc. Am., 86,* 1097-1102.

Collins, M.D., 1990, Benchmark calculations for higher-order parabolic equations, *J. Acoust. Soc. Am., 87,* 1535-1538.

Greene, R.R., 1984, The rational approximation to the acoustic wave equation with bottom interaction, *J. Acoust. Soc. Am., 76,* 1764-1773.

Geoltrain, S. and Brac, J., 1993, Can we image complex structures with first-arrival traveltime?, *Geophysics, 58,* 564-575.

Jensen, F.B., and Ferla, C.M., 1990, Numerical solutions of range-dependent benchmark problems in ocean acoustics, *J. Acoust. Soc. Am., 87,* 1499-1510.

Jensen, F.B., Kuperman, W.A., Porter, M.B. and Schmidt, H., 1994, *Computational Ocean Acoustics*, AIP Press, New York.

Ma, Z., 1982, Steep dip finite difference migration, *Oil Geophysical Prospecting, 1,* 6-15 (in Chinese).

Nichols, D., 1994, Maximum energy traveltimes calculated in the seismic frequency band, *64th SEG Annual Meeting Expanded Abstracts,* 1382-1385.

Podvin, P. and Lecomte, I., 1991, Finite difference computation of traveltimes in very contrasted velocity models: a massively parallel approach and its associated tools, *Geophys. J. Int., 105,* 271-284.

van Trier, J. and Symes, W.W., 1991, Upwind finite-difference calculation of traveltime, *Geophysics, 56,* 812-821.

Vidale, J., 1988, Finite-difference calculation of traveltimes, *Bull. Seism. Soc. Am., 78,* 2062-2076.

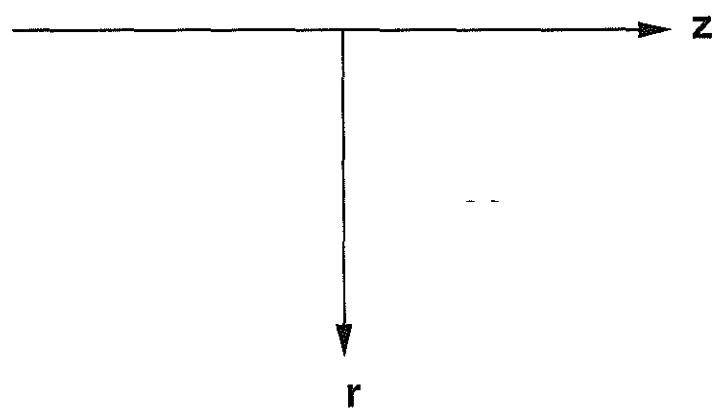

Figure 1: Cylindrical coordinate system

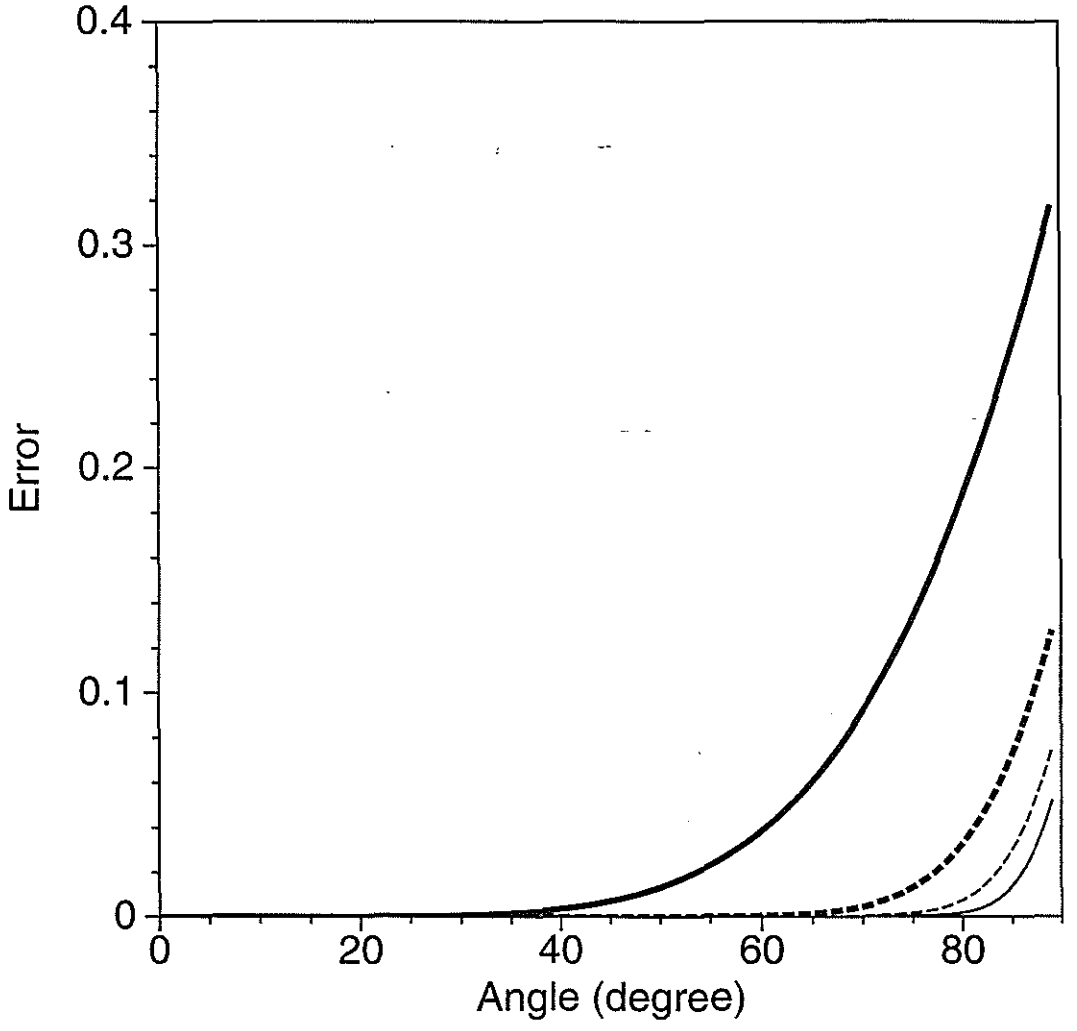

Figure 2: Absolute error versus propagation angle for the Padé series expansion of the square-root operator. The thick solid line is for one term; the thick dashed line is for three terms, the thin dashed line is for five terms; the thin solid line is for seven terms.

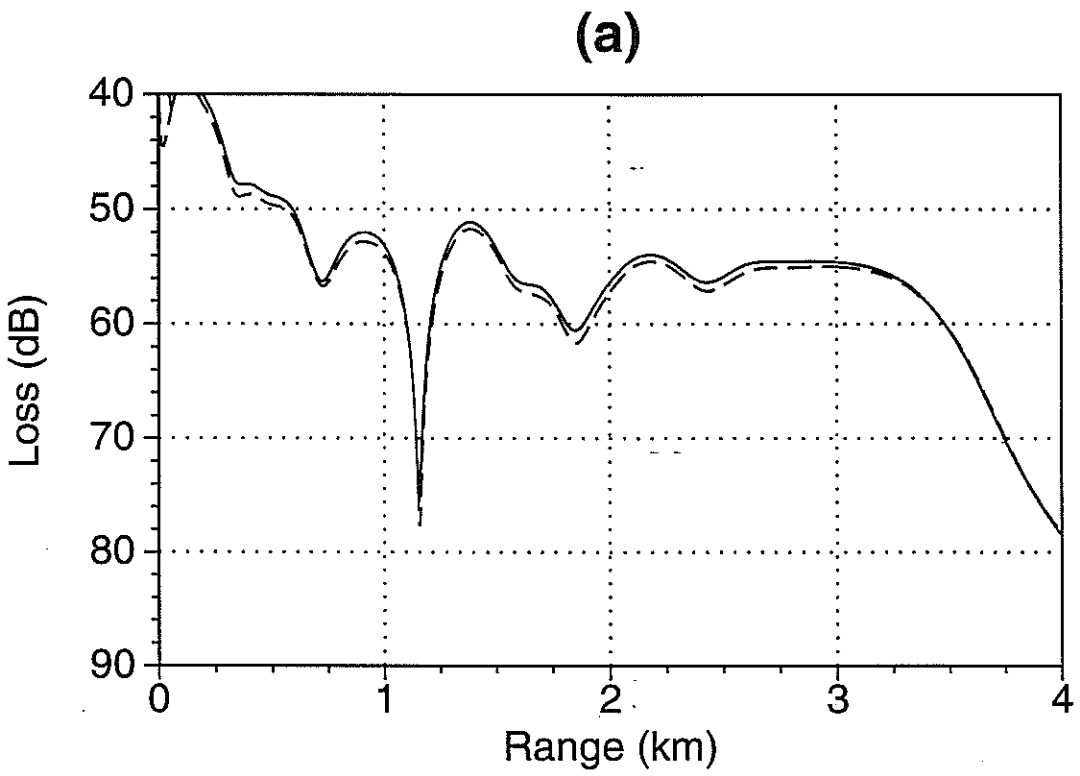

Figure 3: Comparison the transmission loss results (solid line) with the finite element solution (dashed line) for the benchmark wedge problem. (a) Receivers at a depth of 30 m. (b) Receivers at a depth of 150 m.

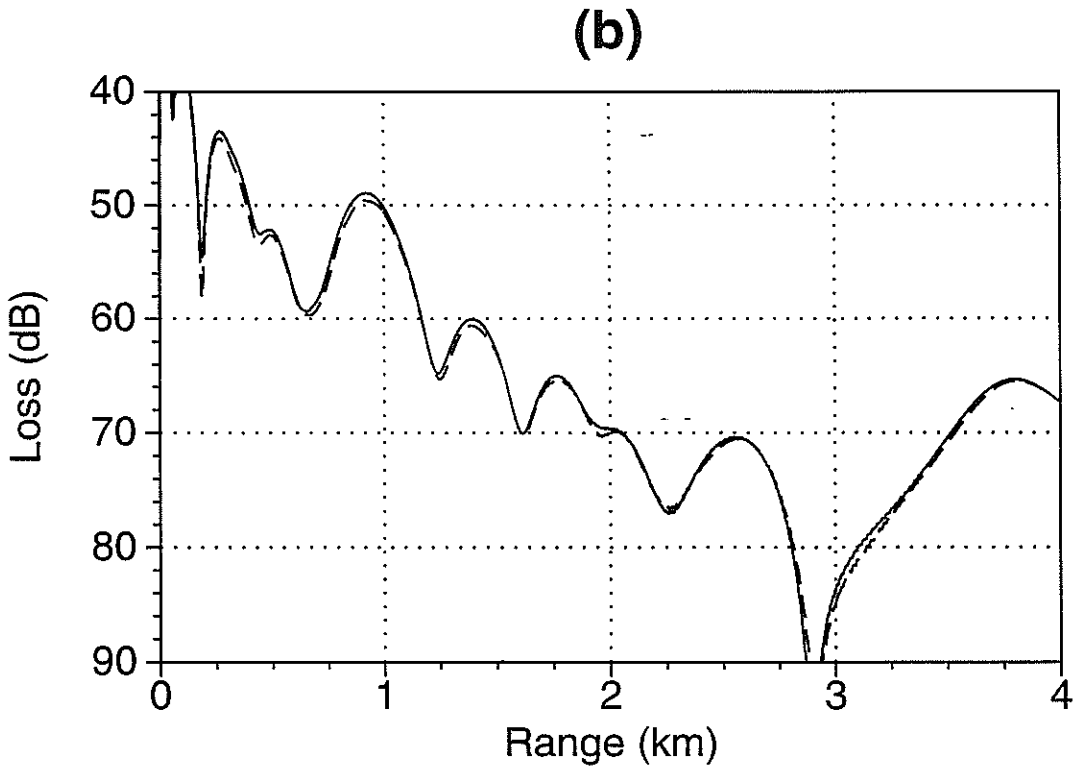

Figure 3, ctd.:

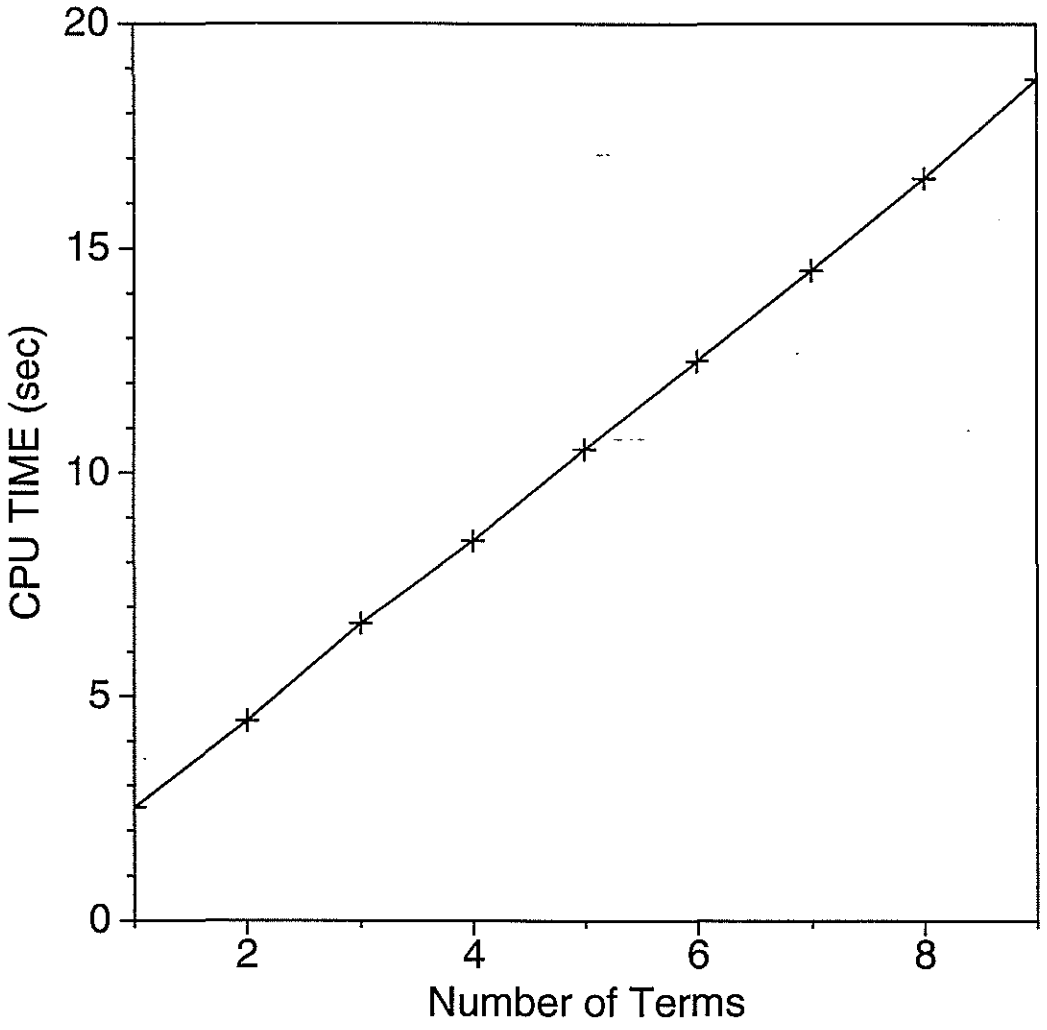

Figure 4: CPU time versus the Padé expansion terms for a 250 × 350 grid model.

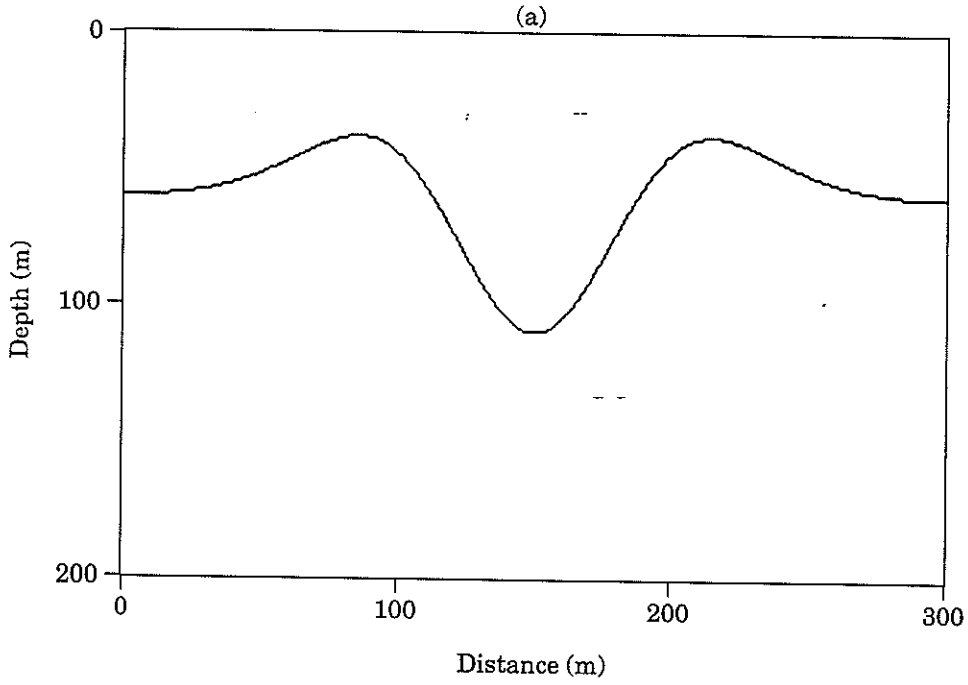

Figure 5: Phase and amplitude results for the syncline model. (a) two layer syncline model. (b) phase plot. (c) amplitude in dB. (d) traveltime contours from graph theory. The layer boundary is indicated by the dashed line.

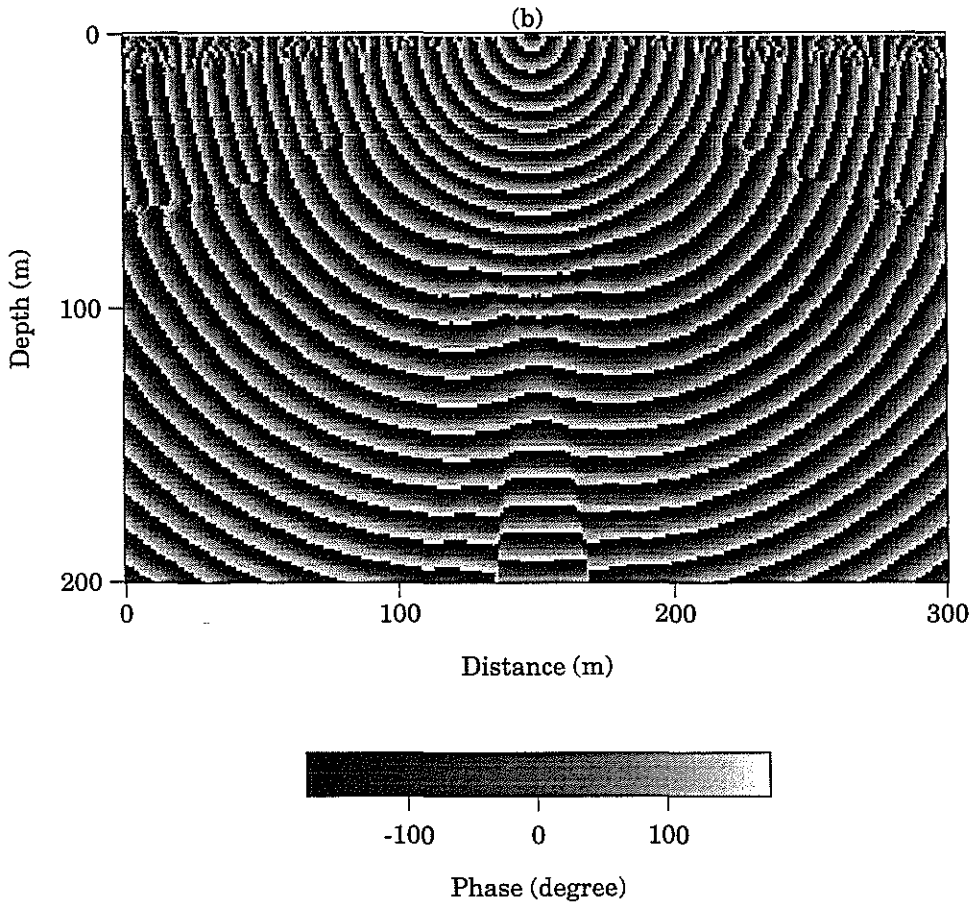
(b)
0
100
200
Depth (m)
0
100
200
300
Distance (m)
-100
0
100
Phase (degree)

Figure 5, ctd.:

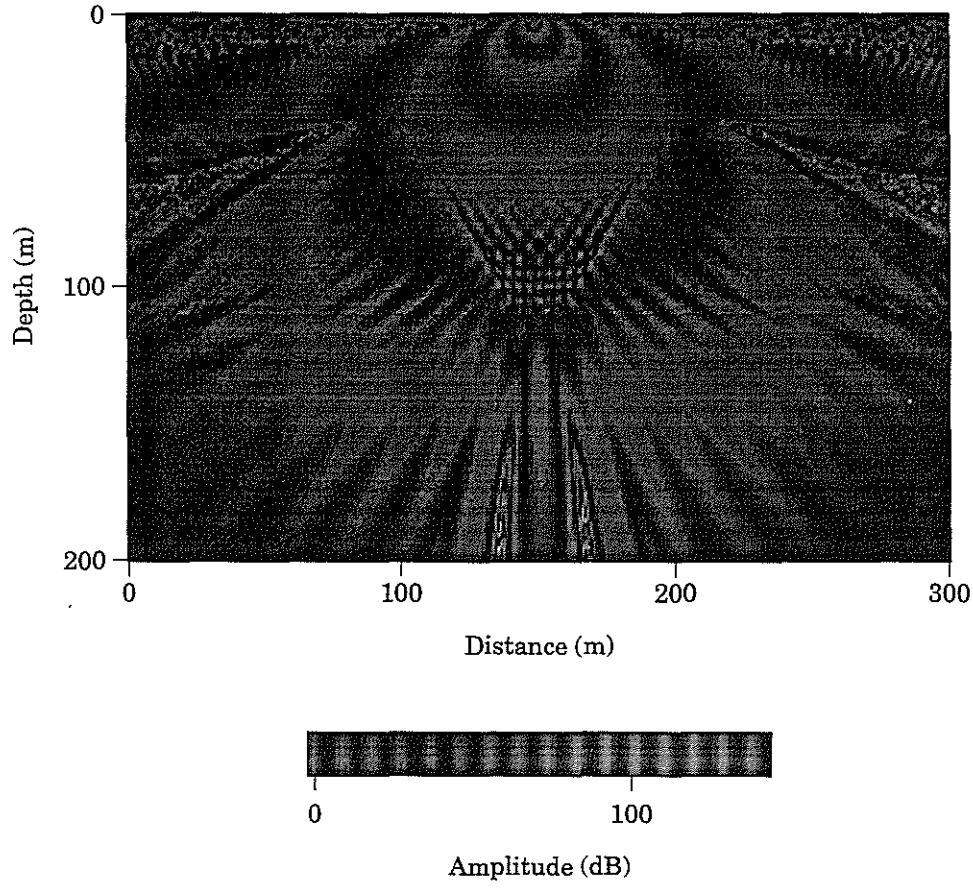

Figure 5, ctd.:

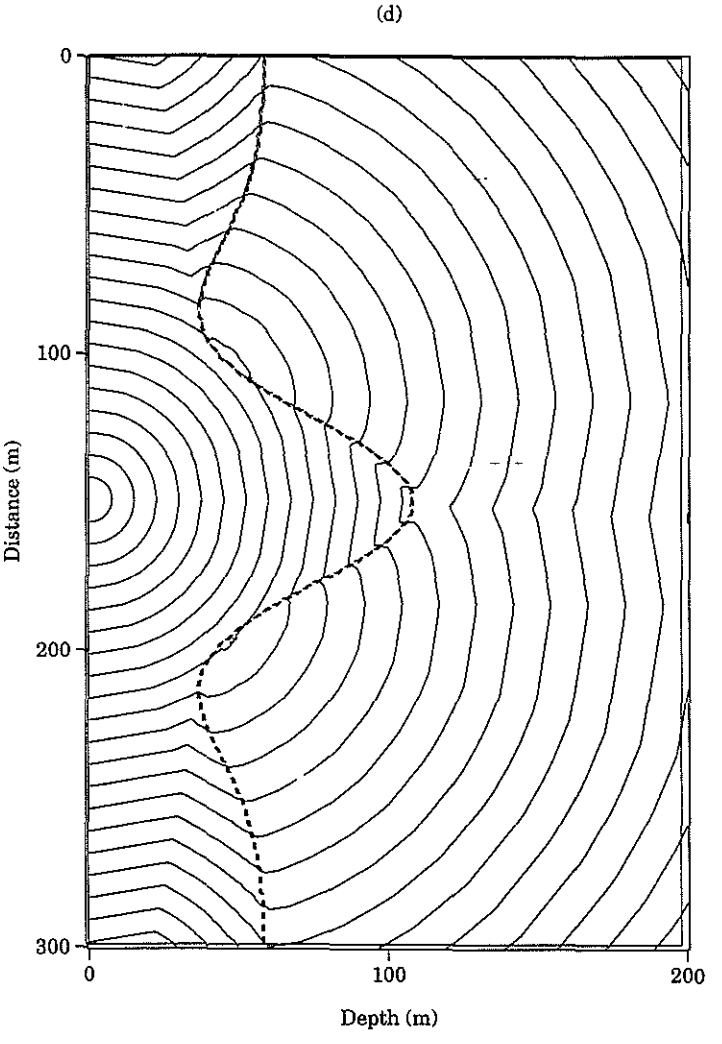

Figure 5, ctd.:

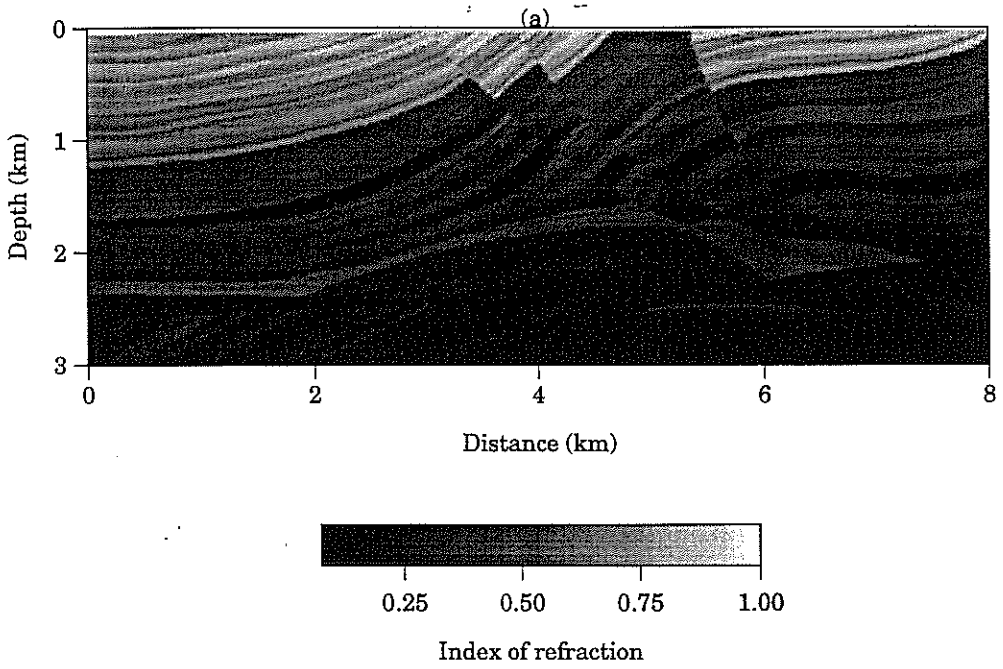

Figure 6: The phase and amplitude results for the Marmousi model. (a) the Marmousi model. (b) phase plot. (c) amplitude in dB.

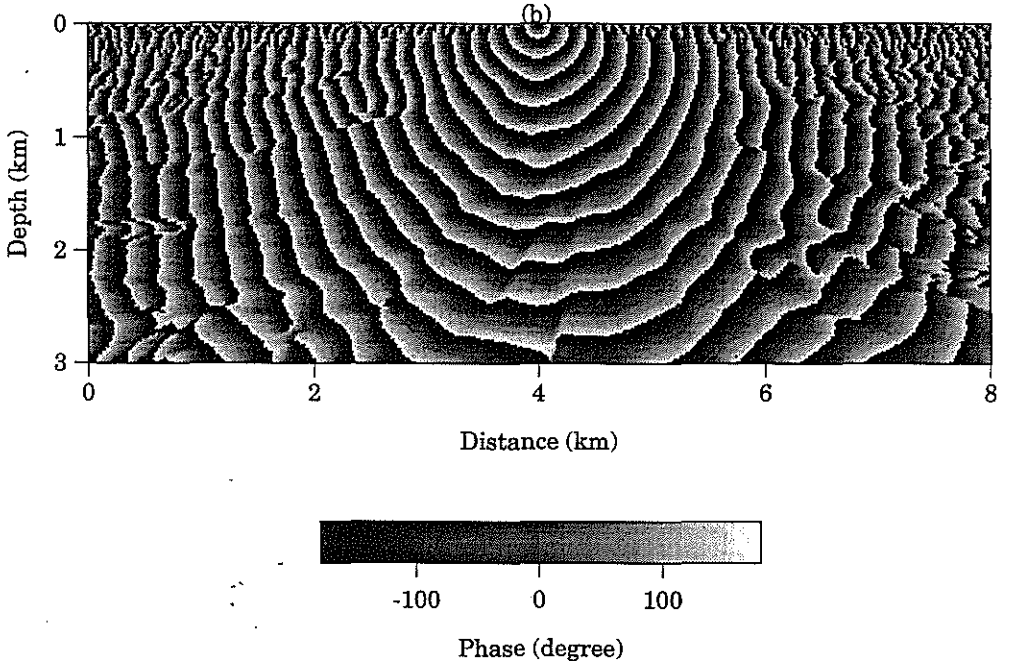

Figure 6, ctd.:

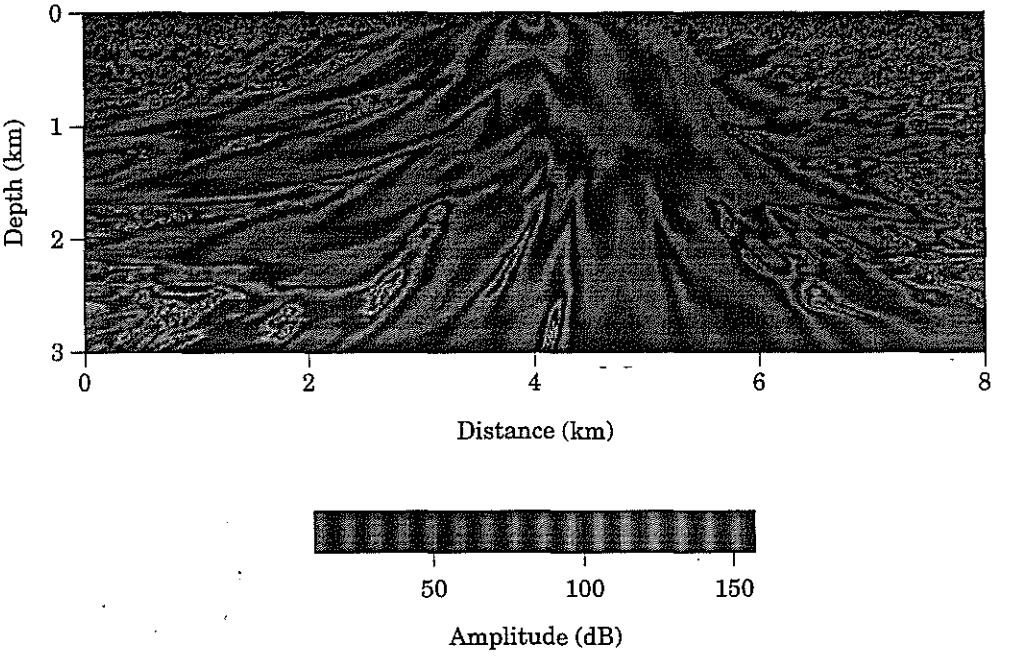

Figure 6, ctd.: